Computer modeling of integrating spheres

Blake G. Crowther

I present a Monte Carlo model for predicting the performance of integrating spheres as a function of incident flux direction. The model was developed specifically to aid in the design of integrating spheres used as cosine collectors but is of general applicability. I discuss a method of generating uncorrelated random numbers. The probability density functions associated with uniform irradiance over a circular entrance port and Lambertian reflectors or emitters are presented. A comparison of the model with analytic equations predicting performance for an unbaffled integrating sphere is included. The average of the data generated by the model agrees with the analytic solution for sphere throughput to better than 0.25% (σ = 8.3%).

Key words: Monte Carlo modeling, integrating sphere, cosine collector, Lambertian reflector.

1. Introduction

Many irradiance measurements require a collector with an angular throughput that is cosinusoidal with the zenith angle of the source. An example of measurements requiring a cosine zenith angle response is the measurement of global solar irradiance at the surface of the Earth. The cosine response is essential in this example if the collector is to imitate perfectly the cosine irradiance falloff experienced at the surface of the Earth as the Sun moves across the sky.[1] A cosine response is especially important when global or all-sky irradiance measurements are made. Any deviation from a cosine response increases the difficulty for proper measurements because of the unknown angular distribution of the diffuse-sky radiance.

At least three different types of cosine collector have been designed and built over the years. One general design type is based on the concept of measuring the light transmitted by a scattering medium such as a plastic resin or frosted glass.[2,3] A typical cosine collector of this type uses a diffuse transmissive material that is shielded around the edges by an opaque material. Once the incident flux passes through the transmissive material, it generally passes into some type of cavity where it is either detected directly or conveyed through a fiber optic to a remote detector. These collectors have shown promise in the visible, but performance is degraded as the wavelength is increased. This degradation with increasing wavelength is due to the wavelength-dependent scattering of the transmissive material. Another method for measuring global irradiance uses a diffuse reflective panel and measures the reflected flux with a nadir-viewing radiometer.[4] A knowledge of the bidirectional reflectance of the panel then allows a correction to be made for the non-Lambertian nature of the panel in the direct portion of the total irradiance. Errors are still present in the global irradiance measurement because the unknown angular distribution of diffuse radiance prohibits a complete correction. A third design approach uses some type of an integrating sphere as the collector. The sphere has an entrance port, an exit port, and usually some type of baffling in the interior.[5] Because integrating spheres inherently are inefficient due to the diffuse scattering nature of the sphere walls, the sphere generally is constructed of, or coated with, some type of highly reflective diffuse material. This approach generally has a greater potential for collecting irradiance over a wider spectral range than the transmissive type of collector and is more accurate than either of the methods mentioned above. However, it is generally less efficient than the other types of cosine collector currently in use.

Several types of integrating-sphere-based cosine collector have been designed and built. Budde[5] discussed three integrating-sphere designs and compared their responses with each other and with the responses of both magnesium oxide and barium-sulfate-coated panels. He found that the spheres outperformed the panels, and that a sphere with an

The author is with the Remote Sensing Group, Optical Sciences Center, University of Arizona, Tucson, Arizona 85721.

Received 13 October 1995; revised manuscript received 6 May 1996.

0003-6935/96/305880-07$10.00/0

annular entrance port and externally baffled exit port exhibited the best angular response. The throughput, defined as the ratio of the flux exiting the exit port to the flux entering the entrance port, of this sphere is quite low at 0.01%. Other researchers successfully used an internal conical baffle in an integrating sphere with a barrier layer cell detector, but Budde[5] was unable to replicate their success with a similar sphere and by imaging the bottom of the baffle onto the entrance slit of a monochromator.

A major difficulty in designing baffled integrating spheres for cosine collectors is the inability of one to arrive at useful closed-form solutions for the angular response of the sphere. Jacquez and Kuppenheim,[6] Goebel,[7] and Finkel[8] developed analytic solutions for determining total reflectance and efficiencies of several different configurations, all without baffling and without consideration for angular response. In principle, integral equations could be developed to predict the angular responses of baffled integrating spheres, but their resultant complexity would prohibit their usefulness in practice. Computer modeling is therefore a logical recourse for predicting the angular response of baffled integrating spheres. A Monte Carlo computer model is presented here. Although the modeling is directed toward a particular application of integrating spheres, the general method can be used for any application. In this paper I present a general theory applicable to modeling integrating spheres, followed by a description of the specific computer model and a test comparison with analytic equations for an unbaffled integrating sphere.

2. Theory

Central to any Monte Carlo modeling effort is a reliable random number generator and the means to transform the uniform distribution on the interval from 0 to 1 [U(0, 1)] into the desired probability density function (PDF).[9] The theory on these topics as applied to this research is presented below.

A. Random Number Generator

The random number generator selected for use in this research was the Sun Microsystems C library function random(), a nonlinear additive feedback random number generator that generates long integers in the range of 0 to $2^{31} - 1$. Its period is approximately $16 \times (2^{31} - 1)$, which is a very large number indeed.[10] The simplest method of generating the U(0, 1) PDF with this random number generator is to divide the number returned by $2^{31} - 1$. This simple method of generating the U(0, 1) PDF was found to be inadequate due to the correlation between two consecutive random numbers. A shuffling routine is therefore used to destroy the consecutive number correlation.[11] The shuffling routine creates an array of numbers and an array pointer, all of which are filled with numbers generated by random(). Each time the routine is called, the pointer indicates which number in the array is to be selected, with the selected number becoming the pointer. The number generated by random() then takes the place of the selected number from the array. Press *et al.* suggest that this method of generating random numbers should be adequate unless the routine from which the original numbers are generated produces nonuniformly distributed numbers.[11]

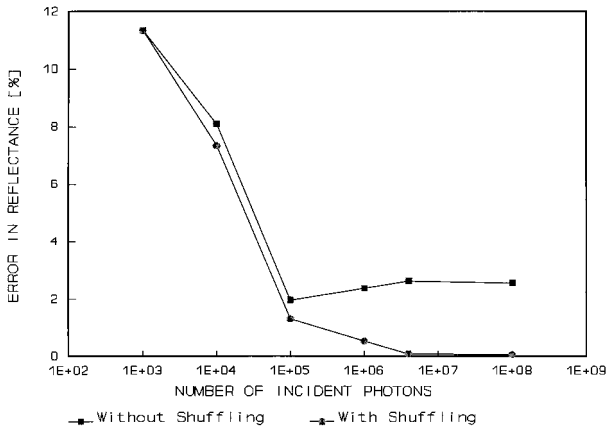

Fig. 1. Errors in the predicted reflectance at the air–fiber interface with and without shuffling. Computations were done at normal incidence with a fiber index of refraction of 1.46.

The effectiveness of the shuffling routine in destroying the correlation was tested by a comparison of the reflectance of the nonshuffled with shuffled routines at normal incidence at an air–fiber interface with an index of refraction of 1.46. The method of determining the transmission or reflection of a photon, discussed in detail in Subsection 2.C, involves the comparison of two consecutive random numbers. It therefore provides an excellent test for the correlation between consecutive numbers generated with any pseudorandom number generator. For Fig. 1, no shuffling was used to generate the top curve, but the bottom curve was generated with the shuffled routine. The error in reflectance seemed to stabilize at approximately 2.5% without shuffling and asymptotically approached zero with shuffling.

B. Probability Density Functions

To generate random numbers that simulate observed phenomena, they must be extracted from the appropriate PDF. Therefore the PDF must be known, and the numbers drawn from the available U(0, 1) PDF must be transformed into the correct PDF. The general procedure for transforming the U(0, 1) PDF into the desired PDF was published previously by Frieden.[9] The procedure reduces to the transformation equation shown in Eq. (1), where u is a number drawn from the U(0, 1) PDF, $F(c)$ is the cumulative probability function, and $p_c(c)$ is the PDF:

$$u = F(c) \equiv \int_{-\infty}^{c} p_c(c')\mathrm{d}c'. \tag{1}$$

In this model, the PDF required to produce uniform entrance port irradiance and the PDF required to produce an intensity distribution following Lambert's

cosine law were developed. Equation (2) is Lambert's cosine law that relates the intensity I at a particular zenith angle θ to the intensity I_0 at a zenith angle of zero. Any surface obeying this law is called Lambertian[1]:

$$I(\theta) = I_0 \cos(\theta). \tag{2}$$

To test the angular response of an integrating sphere, a photon is introduced through the entrance port of the sphere at a random position, implying uniform irradiance over the entrance port. A method of generating uniformly distributed photon entrance points over the area of the entrance port of the modeled integrating spheres was required to simulate the uniform irradiance condition. This requires that two coordinates, either r and θ or x and y, be selected. The coordinates x and y are the most convenient descriptors of the photon entrance position because the motion of the photon is most easily described in rectilinear coordinates. Therefore if r and θ are generated from the U(0, 1) PDF, a transformation to x and y is necessary. Because the irradiance is constant, the total number of photons entering a circular aperture of arbitrary radius is calculated easily with Eq. (3), assuming that the irradiance is monochromatic:

$$N(r) = \pi r^2 E/h\nu, \tag{3}$$

where E represents the constant irradiance, r is the radius, ν the photon frequency, N the number of photons, and h is Planck's constant. Once the total number of photons entering a circle of radius r is known, the cumulative distribution function can be written immediately with Eq. (4):

$$F(r) = r^2/R^2, \tag{4}$$

where R is the radius of the entrance port. The PDF is the derivative of the cumulative distribution function and is shown in Eq. (5):

$$p(r) = 2r/R^2. \tag{5}$$

Either $p(r)$ or $F(r)$ can be used to transform the numbers drawn from U(0, 1) into the desired PDF. The more convenient of the two is $F(r)$ because the integration of $p(r)$ is one step in the process. Labeling the random variable drawn from the U(0, 1) PDF as u and solving the transformation equation yields Eq. (6):

$$r = R\sqrt{\mathrm{u}}. \tag{6}$$

The irradiance incident on the entrance port shows no preference for one angular region over the other, so the PDF for θ is just a uniform distribution for the region of 0–2π. One can transform the numbers drawn from the available U(0, 1) PDF to the PDF for θ by simply multiplying by 2π. With the relationship between r and θ and x and y, the final equations for the generation of x and y, which will produce uniform entrance port irradiance, are shown in Eqs. (7) and (8), where u and v represent numbers drawn from the U(0, 1) PDF:

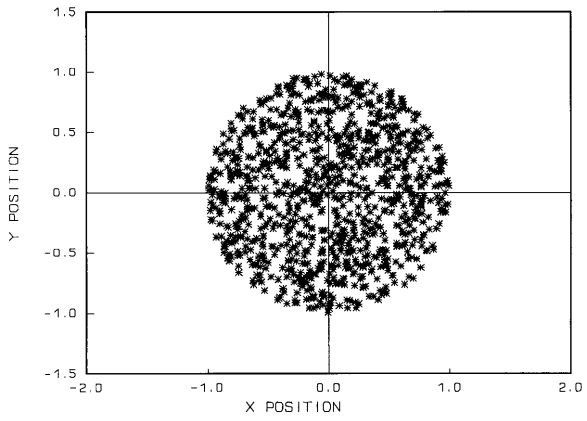

Fig. 2. Photon entrance points resulting from randomly generating x and y coordinates and throwing away those points outside the entrance aperture. A total of 1000 points were generated, and an entrance aperture of radius 1 unit was used.

$$x = R\sqrt{u}\cos(2\pi v), \tag{7}$$

$$y = \mathrm{R}\sqrt{u}\sin(2\pi v). \tag{8}$$

The other possibility for producing uniform irradiance inside a circular aperture is a brute-force approach, in which both x and y are extracted from the $1/R$*U(0, R) PDF, and points lying outside the circle of radius R are thrown away. Approximately 21.5% of all the points generated are discarded following this method. Somewhat surprisingly, no appreciable difference in execution time was noted between the two methods. This similarity in execution time can be attributed to the relatively long time required to compute the trigonometric functions. The results of both methods can be seen in Figs. 2 and 3.

The interior surfaces of the integrating sphere and baffle surfaces, if applicable, were modeled as Lambertian surfaces. Directions for photons reflected from these surfaces are required to be chosen from PDF's such that Eq. (2) is satisfied. PDF's for the

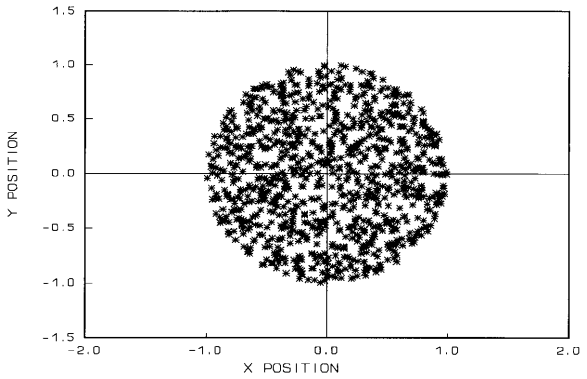

Fig. 3. Photon entrance points resulting from the use of transformation Eqs. (7) and (8) to generate the x and y coordinates. A total of 1000 points were generated, and an entrance aperture of radius 1 unit was used.

azimuth angle ϕ and the zenith angle θ were developed to give reflected photons the correct direction.

Because Lambert's cosine law is independent of the azimuth angle, photons can be reflected in any azimuth direction with equal probability. The proper azimuth PDF is therefore just the uniform PDF over the interval $0–2\pi$. To transform the numbers generated from the U(0, 1) PDF to the proper azimuthal PDF, one can multiply the number generated by 2π.

The total flux Φ reflected within the zenith angle range $0–\theta$ by a Lambertian reflector can be found when one integrates the intensity distribution in Eq. (2) over the solid angle subtended at the angle θ as shown in Eq. (9):

$$\Phi(\theta) = \int_{\phi'=0}^{2\pi} \int_{\theta'=0}^{\theta} I_0 \cos(\theta')\sin(\theta')\mathrm{d}\theta'\mathrm{d}\phi' = I_0\pi \sin^2(\theta). \tag{9}$$

The zenith angle corresponding to an entire hemisphere is 90°, resulting in a total reflected flux of πI_0 W. Flux levels are converted to monochromatic photon counts when one divides the flux by Planck's constant and the frequency, which yields the total number of photons emitted within the zenith angle range $0–\theta$. When this is divided by the total number of photons emitted for the entire hemisphere, it yields the cumulative probability distribution in Eq. (10):

$$F(\theta) = \sin^2(\theta). \tag{10}$$

Differentiating $F(\theta)$ with respect to θ, yields Eq. (11):

$$p(\theta) = 2 \sin(\theta)\cos(\theta). \tag{11}$$

An independent method of finding $p(\theta)$ developed in consultation with Frieden[12] gives the same result. Once again the transformation equation, letting u be the number extracted from the U(0, 1) PDF, is applied as shown in Eq. (12):

$$u = F(\theta) = \sin^2(\theta). \tag{12}$$

Solving for θ yields Eq. (13), which can be applied to the numbers generated by the U(0, 1) PDF.

$$\theta = a \sin(\sqrt{u}). \tag{13}$$

C. Photon Reflection Techniques

One can determine the possibility of a photon being reflected at an air–fiber interface by first calculating a polarization angle according to the U(0, 2π) PDF, with the polarization angle of 0 being defined as p polarized. In this research p polarization is referred to as electromagnetic radiation in which the oscillations of the electric field are parallel to the plane of incidence, and s polarization is referred to as radiation in which the oscillations of the electric field are perpendicular to the plane of incidence. The p and s reflectances are then calculated with the standard Fresnel formulas in Eqs. (14) and (15)[13]:

$$r_p = \frac{n_t \cos(\theta_i) - n_i \cos(\theta_t)}{n_t \cos(\theta_i) + n_i \cos(\theta_t)}, \tag{14}$$

$$r_s = \frac{n_i \cos(\theta_i) - n_t \cos(\theta_t)}{n_i \cos(\theta_i) + n_t \cos(\theta_t)}. \tag{15}$$

The symbols n_i and n_t refer to the incident and transmitted index of refraction, respectively, and θ_i and θ_t refer to the incident and transmitted angles, respectively. These component electric-field reflectances are combined appropriately in Eq. (16) and yield a reflectance that is valid for irradiance at a particular polarization angle and incident angle[13]:

$$R = r_p^2 \cos^2(\theta_p) + r_s^2 \sin^2(\theta_p). \tag{16}$$

In this case, θ_p refers to the polarization angle. A random number from the U(0, 1) PDF is compared with this reflectance and the photon reflected if the number is less than or equal to the reflectance.

The method of determining the absorption of a photon at the surface of the diffuse sphere wall and baffle surfaces is much simpler because these surfaces are modeled as Lambertian. The absence of specular reflection allows the possibility of absorption to be determined by a comparison of a random number from the U(0, 1) PDF to the value for the reflectance without concern for polarization and incident angles. Once again, if the number drawn from the U(0, 1) PDF is less than or equal to the reflectance, then the photon is reflected.

3. Model Description

The theory described above and the general procedure of tracing the complex path of a photon within the integrating sphere are applicable to any Monte Carlo sphere model. The validity of the model is tested by a comparison of the modeled data with the predictions of analytic equations for an unbaffled sphere with an attached fiber-optic cable.

A. General Model Procedure

The user specifies the dimensions of the sphere, entrance port, exit port, and baffles, as well as the desired photon entrance directions. It is assumed that a fiber-optic cable is used in the exit port so that a numerical aperture (NA) and an index of refraction (n) are also specified by the user. This is not a limitation because values of 1 NA and $n = 1$ can be used for the case in which no fiber exists at the exit port. The user also specifies photon entrance directions, from which direction cosines are calculated.

The photon entrance position within the entrance port is chosen according to the theory described above. This entrance point, combined with the direction cosines, yields parametric Eqs. (17), (18), and

(19), describing the linear motion of the photon:

$$x_1 = x_0 + \alpha t, \tag{17}$$

$$y_1 = y_0 + \beta t, \tag{18}$$

$$z_1 = z_0 + \gamma t, \tag{19}$$

where subscript 1 denotes the new position coordinate, and subscript 0 denotes the original coordinate position. The x-direction cosine is given by α, the y-direction cosine by β, the z-direction cosine by γ, and t is the common parameter. These parametric equations are used, along with equations describing the geometry of the internal surfaces, to find solutions for parameter t. The solutions for t are then substituted into the parametric equations to find the intersections of the photon path with the sphere wall and other internal surfaces. These intersection points are checked against the limits of the internal surfaces, and the point is disqualified if it lies outside the surface boundaries. An intersecting point is also disqualified if t is negative or so close to the origination point that it is judged to be the same point. The collision point is selected as the intersection point associated with the smallest value of t.

Once the collision point is known, four possible conditions for which the lifetime of the photon within the sphere expires are examined. The first two conditions are simple, and the latter two are relatively complex. One condition consists of checking to assure that a predetermined number of maximum collisions is not exceeded, guarding against an infinite loop. The second photon expiration condition is that of escape by way of the entrance port. Here, the collision point is examined to see if it lies on the part of the sphere corresponding to the entrance port. At least one collision is required before a photon can escape out the entrance port because the initial direction of travel is to enter the entrance port.

The possibility of a photon colliding with the fiber face at the exit port is examined next. If a collision at the air–fiber interface does occur, several other checks must be made. First, the polarization of the photon is determined and the reflectance calculated as described previously. In the event of transmission into the fiber, a calculation is made to check if the photon is traveling within the specified NA of the fiber. If the transmitted photon is within the fiber NA, then it is counted as having been transmitted by the fiber to the detector. The event of Fresnel reflection requires that a new set of direction cosines be calculated according to the laws of specular reflection. The only direction cosine to require modification in this case is the one corresponding to the perpendicular to the fiber face. The modification consists of one negating that particular direction cosine, after which the process is repeated, beginning with the determination of new parametric equations. The only difference is that the direction cosines and point of origination have been calculated by the program instead of being supplied by the user.

The final photon expiration condition to be examined is that of absorption of the photon by the walls of the sphere or baffles. If the calculation reveals that the photon is not absorbed, then new direction cosines are calculated in the local coordinates according to the law of reflectance obeyed by a Lambertian reflector. The sphere axes are constructed such that the z axis passes through the center of the entrance port and the x axis passes through the center of the exit port on the side of the sphere, if an exit port exists at that location. If no defining features exist, then the choice of direction for the x axis is arbitrary. The x axis always corresponds to a zenith angle of 90° and the z axis a zenith angle of 0°. The local axes are chosen such that the local z direction corresponds to the sphere $-r$ direction (which is the outward normal of the inside of the sphere), the local y direction corresponds to the sphere ϕ direction, and the local x direction corresponds to the sphere $-\theta$ direction. These local or primed coordinates are expressed in terms of the sphere coordinates in Eqs. (20), (21), and (22)[14]:

$$\hat{\mathbf{x}}' = -\hat{\boldsymbol{\theta}} = -\cos(\theta_{\alpha x})\cos(\phi_{\alpha x})\hat{\mathbf{x}} - \cos(\theta_{\alpha x})\sin(\phi_{\alpha x})\hat{\mathbf{y}} + \sin(\theta_{\alpha x})\hat{\mathbf{z}}, \tag{20}$$

$$\hat{\mathbf{y}}' = \hat{\boldsymbol{\phi}} = -\sin(\phi_{\alpha x})\hat{\mathbf{x}} + \cos(\phi_{\alpha x})\hat{\mathbf{y}}, \tag{21}$$

$$\hat{\mathbf{z}}' = -\hat{\mathbf{r}} = -\sin(\theta_{\alpha x})\cos(\phi_{\alpha x})\hat{\mathbf{x}} - \sin(\theta_{\alpha x})\sin(\phi_{\alpha x})\hat{\mathbf{y}} - \cos(\theta_{\alpha x})\hat{\mathbf{z}}. \tag{22}$$

The new or primed direction cosines are calculated from the local azimuth and zenith angles generated from the governing Lambertian reflector PDF's. The local direction cosines are then transformed into the sphere coordinates by one dotting the sphere axes with the local or primed axes in Eqs. (23), (24), and (25):

$$\alpha = \hat{\mathbf{x}} \cdot \hat{\mathbf{x}}'\acute{\alpha} + \hat{\mathbf{x}} \cdot \hat{\mathbf{y}}'\acute{\beta} + \hat{\mathbf{x}} \cdot \hat{\mathbf{z}}'\acute{\gamma}, \tag{23}$$

$$\beta = \hat{\mathbf{y}} \cdot \hat{\mathbf{x}}'\acute{\alpha} + \hat{\mathbf{y}} \cdot \hat{\mathbf{y}}'\acute{\beta} + \hat{\mathbf{y}} \cdot \hat{\mathbf{z}}'\acute{\gamma}, \tag{24}$$

$$\gamma = \hat{\mathbf{z}} \cdot \hat{\mathbf{x}}'\acute{\alpha} + \hat{\mathbf{z}} \cdot \hat{\mathbf{y}}'\acute{\beta} + \hat{\mathbf{z}} \cdot \hat{\mathbf{z}}'\acute{\gamma}. \tag{25}$$

The direction cosines are now known in the sphere coordinates, and the collision point becomes the new origin point. Therefore the process begins again with new parametric equations. Just as in the case of the specular reflection above, the direction cosines and origin point are calculated by the program instead of being supplied by the user.

The process just described is repeated for as many photons as desired at each entrance angle. The process is intense computationally but gives reasonable predictions without building and testing candidate spheres.

B. Model Example

The first sphere model is a 10.16-cm-diameter sphere with a diffuse reflectance of 0.99. A 2.54-cm-diameter entrance port is located at the top of the sphere, perpendicular to the z axis. The axis of the exit port is located at a 90° angle from the axis of the entrance port, along the x-sphere axis. A fiber-optic

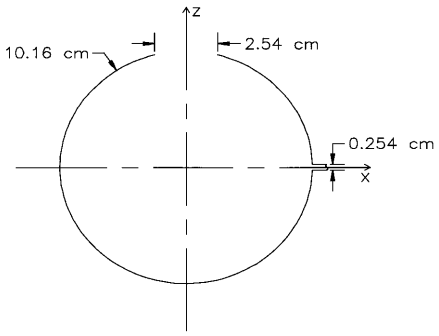

Fig. 4. Unbaffled integrating sphere with an incorporated fiber-optic cable at the exit port. The axes of the entrance and exit ports correspond to the z and x axis, respectively.

cable with a diameter of 0.254 cm, a NA of 0.28 (half-field view angle of 16.26°), and an index of refraction equal to 1.46 is coupled to the exit port. No baffling is used with this sphere design. This sphere is shown as a cross section in Fig. 4.

The sphere model was tested at zenith angles of 0° through 80° in 10° increments. Azimuth angles of 0° through 345° in 15° increments were used at each of the zenith angles except 0°, where the azimuth angle is irrelevant. A total of 10^6 photons were traced at each zenith and azimuth angle combination. This resulted in an effective irradiance increase of $1/\cos(\theta)$, so the output of the sphere should have remained constant at all incident angles if it were a true cosine collector. Several photons were traced by hand to verify that the model functioned as designed before the final tests were run.

4. Results

The number of photons entering the fiber-optic cable is graphed as a function of azimuth angle at zenith angles of 10° through 80° in Figs. 5, 6, and 7. Figure 5 shows that the output of the sphere remains relatively constant at zenith angles of 10° through 30°. The output is highly nonuniform at zenith angles of

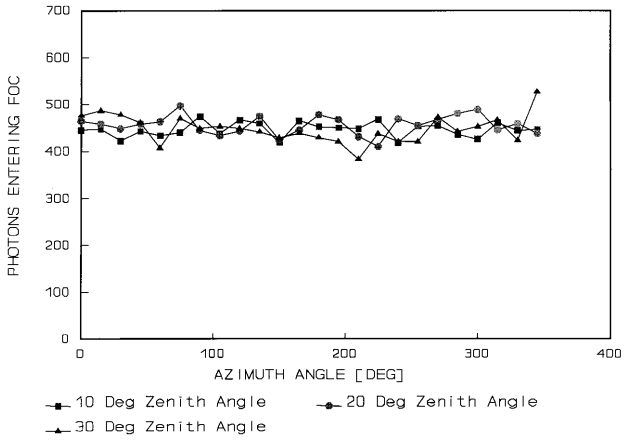

Fig. 5. Photons entering the fiber-optic cable of the unbaffled sphere as a function of azimuth angle at zenith angles of 10°, 20°, and 30°. 10^6 photons were traced at each input direction.

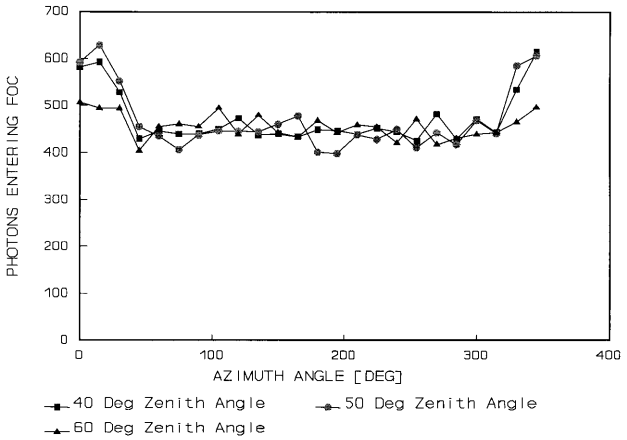

Fig. 6. Photons entering the fiber-optic cable of the unbaffled sphere as a function of azimuth angle at zenith angles of 40°, 50°, and 60°. 10^6 photons were traced at each input direction.

40° and 50°, and slightly nonuniform at 60° as shown in Fig. 6. This nonuniformity is a result of the unsymmetric nature of the sphere with respect to azimuth angle. The exit port and fiber are placed at zenith angles of 90° along the x axis as shown in Fig. 4. This construction allows a clear view of the opposite side of the sphere along the $-x$ axis. In fact, photons must originate from a point within the selected NA to enter the fiber. The photons that collide with the sphere wall opposite the exit port on the first collision, therefore, have a higher probability of entering the fiber than photons that collide with other portions of the sphere on the first collision. As expected, the output became more constant as the zenith angle was increased, as shown in Fig. 7.

The output of a basic sphere such as the one discussed above can also be estimated with Eq. (26)[15]:

$$\Phi_{pf} = \frac{\rho \Phi_{pep} A_f (\mathrm{NA})^2 (1 - R)}{A_s \left\{ 1 - \rho \left[1 - \left(\frac{A_f + A_{ep}}{A_s} \right) \right] \right\}}, \tag{26}$$

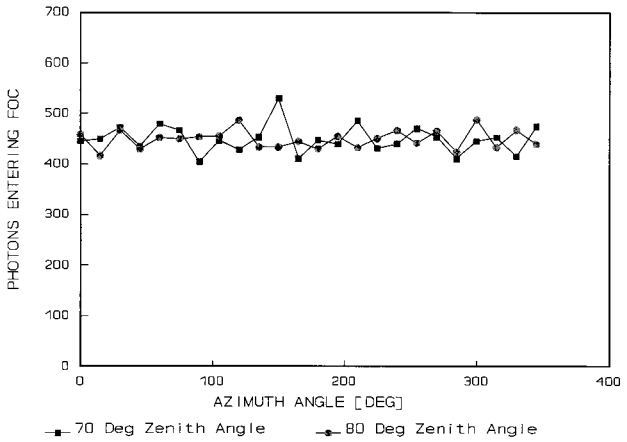

Fig. 7. Photons entering the fiber-optic cable of the unbaffled sphere as a function of azimuth angle at zenith angles of 70° and 80°. 10^6 photons were traced at each input direction.

Table 1. Statistics on the Number of Photons Entering the Fiber-Optic Cable[a]

Zenith Angle (deg)	Average	Standard Deviation	Percent Difference
0	429	n/a[b]	−6.02
10	446.17	15.45	−2.26
20	455.96	20.87	−0.12
30	447.13	29.99	−2.05
40	471.58	55.56	+3.30
50	469.21	68.58	+2.78
60	456.79	27.39	+0.06
70	449.04	27.92	−1.63
80	448.38	18.51	−1.78

[a]The statistics for all zenith angles except 0° include azimuth angles 0° through 345° at 15° increments. At 0°, the azimuth angle used was 0°.
[b]n/a means not available.

where Φ_{pf} is the photon flux entering the fiber, ρ is the sphere wall diffuse reflectance (0.99), Φ_{pep} is the photon flux entering the entrance port (10^6), A_f is the cross-sectional area of the fiber (0.0507 cm^2), NA is the numerical aperture (0.28), R is the fiber reflectance (estimated as the Fresnel reflectance at normal incidence of 0.035), A_s is the surface area of the sphere (324.29 cm^2), and A_{ep} is the area of the entrance port (5.067 cm^2). The calculation of Eq. (26) yields an estimated output photon flux of 456.5 photons. This estimate assumes the photons hit the wall of the perfectly diffusely reflecting sphere but does not take into account any directionality. The average number of photons entering the fiber-optic cable at each zenith entrance angle is listed in Table 1 along with the standard deviation and the percent difference from the 456.5 photon estimate. The average number of photons entering the fiber from all the zenith and azimuth angle combinations is perhaps the best comparison with the analytic results because the directionality is nullified by the averaging. The overall average estimated by the model is calculated to be 455.4, with a standard deviation of 37.9. Thus the overall average of the model results in a difference of −0.24% from the theoretical estimate.

5. Conclusions

Extensive effort has been applied to derive analytical solutions for performance criteria of integrating spheres over the years. Closed-form mathematical solutions for throughput as a function of incident angle have not been derived even for simple integrating spheres. Because of the unavailability of closed-from mathematical equations to evaluate baffled integrating spheres, designs must be based on modeling or experimentation. Monte Carlo modeling can be used to predict the angular throughput, thereby guiding integrating sphere design. I used such modeling techniques successfully to model several integrating spheres coupled with fiber-optic cables. The model predictions of baffled spheres will require experimental verification from designs currently under construction. The basic integrating sphere modeled for this research was compared with theory, with excellent results that are consistent with the predictions of analytic equations developed in earlier research to better than 0.25% overall.

Appreciation is expressed to the faculty, staff, and students at the Remote Sensing Group, Optical Sciences Center, University of Arizona, for helpful discussions concerning this research. This research was conducted under NASA Graduate Student Researchers Program fellowship grant NGT-51219 and NASA contract NAS5-31717.

References

1. P. N. Slater, *Remote Sensing: Optics and Optical Systems* (Addison-Wesley, Reading, Mass., 1980).
2. L. Harrison, J. Michalsky, and J. Berndt, "Automated multifilter rotation shadow-band radiometer: an instrument for optical depth and radiation measurements," Appl. Opt. **33,** 5118–5125 (1994).
3. R. M. Schotland and J. D. Copp, "Optical properties of a plastic pyranometer head," J. Appl. Meteorol. **21,** 735–739 (1982).
4. S. F. Biggar, P. N. Slater, and D. I. Gellman, "Uncertainties in the in-flight calibration of sensors with reference to measured ground sites," Remote Sensing Environ. **48,** 245–252 (1994).
5. W. Budde, "Integrating sphere for the photometry of the sky," Appl. Opt. **3,** 939–941 (1964).
6. J. A. Jacquez and H. F. Kuppenheim, "Theory of the integrating sphere," J. Opt. Soc. Am. **45,** 460–470 (1955).
7. D. G. Goebel, "Generalized integrating-sphere theory," Appl. Opt. **6,** 125–128 (1967).
8. M. W. Finkel, "Integrating sphere theory," Opt. Commun. **2,** 25–28 (1970).
9. R. Frieden, *Probability, Statistical Optics and Data Testing: a Problem Solving Approach* (Springer-Verlag, New York, 1991).
10. SunOS Reference Manual, Sun Release 4.1, 1990, Vol. II, Sect. 3, p 3–255.
11. W. H. Press, B. P. Flannery, S. A. Teukolsky, and W. T. Vetterling, *Numerical Recipes in C* (Cambridge U. Press, New York, 1988), Chap. 7.
12. B. R. Frieden, Optical Sciences Center, University of Arizona, Tucson, Arizona 85721 (personal communication, 1993).
13. M. Born and E. Wolf, *Principles of Optics*, 6th ed. (Pergamon, New York, 1989), Chap. 1, pp. 36–47.
14. R. K. Wangsness, *Electromagnetic Fields*, 2nd ed. (Wiley, New York, 1986), Chap. 1.
15. K. F. Carr, "Integrating sphere calibration sources for remote sensing imaging radiometers," in *Optical Radiation Measurements II*, J. M. Palmer, ed., Proc. SPIE **1109,** 99–113 (1989).